AIAA JOURNAL
Vol. 40, No. 12, December 2002

Chaos in a Thermally Stressed Space Arc

Lazarus Teneketzis Tenek*
Aristotle University of Thessaloniki, GR-541 24 Thessaloniki, Greece

A three-dimensional isotropic space arc that is subjected to an oscillating temperature is considered. The latter is equal to its critical temperature with a slight sinusoidal variation. A dynamic nonlinear finite element problem is formulated and solved by means of an unconditionally stable time-dependent scheme. Highly irregular time-displacement curves are obtained for a midarc point. The horizontal displacement of the midarc point from the onset of the vibration is highly oscillatory. In addition, the trajectory of the midpoint in space is chaotic. Two- and three-dimensional attractors are given. To prove the chaotic nature of the motion, the fast Fourier transform and the Lyapunov exponent of the vertical movement of the center point are provided. Both prove the chaotic nature of the arc vibration. Computer plots of the arc deformation at two time instances show the structural deformation and the possible catastrophic collapse.

Nomenclature

a_N	=	transformation matrix between elemental natural and global Cartesian coordinates
$\bar{a}_N$	=	connection matrix between elemental natural and local Cartesian coordinates
C	=	global damping matrix
$\boldsymbol{F}_N$	=	natural elemental force vector due to axial straining mode
$\boldsymbol{J}$	=	initial load vector due to temperature
$\boldsymbol{J}_N$	=	natural thermal elemental load vector
$\boldsymbol{J}_{N0}, \boldsymbol{J}_{N1}$	=	thermal elemental load vector due to uniform temperature distribution and due to linear through-the-thickness temperature distribution
K, K_E, K_G	=	global tangent, elastic, and geometric stiffness matrices
M	=	global mass matrix
M_A^1, M_A^2	=	antisymmetrical elemental natural bending moment in the $x'z'$ and $x'y'$ planes
M_S^1, M_S^2	=	symmetrical elemental natural bending moment in the $x'z'$ and $x'y'$ planes
M_T	=	elemental natural torsional moment in the $y'z'$ plane
$\boldsymbol{P}_N$	=	natural force elemental vector due to straining modes
$\boldsymbol{P}_0$	=	elemental vector due to natural rigid body modes
P_{01}, P_{02}, P_{03}	=	translational rigid-body force along the x', y', and z' local elemental axes
P_{04}, P_{05}, P_{06}	=	rotational rigid-body moment with respect to the x', y', and z' local elemental axes
$\boldsymbol{p}_s, \boldsymbol{p}_{VD}$	=	vectors of surface tractions and of distributed damping forces
$\boldsymbol{R}$	=	external force vector
$\boldsymbol{R}_D$	=	damping vector
$\boldsymbol{R}_E, \boldsymbol{R}_1$	=	vectors of elastic forces and inertial forces
$\boldsymbol{r}_k$	=	displacement vector at iteration k
$\boldsymbol{r}_{k,t}$	=	velocity vector at iteration k
$\boldsymbol{r}_{k,tt}$	=	acceleration vector at iteration k
$\boldsymbol{r}_{k,ttt}$	=	first derivative of acceleration vector at iteration k
T_0	=	half the sum of the top and bottom beam temperatures
T_1	=	difference of the top and bottom beam temperatures divided by thickness
u, v, w	=	displacements along the global x axis, global y axis, and global z axis
$\dot{w}$	=	velocity along the global z axis
$\ddot{w}$	=	acceleration along the global z axis
γ	=	strain vector
Δt	=	time step
ε	=	convergence tolerance
ρ	=	density
$\boldsymbol{\rho}$	=	vector containing the natural modes
$\bar{\boldsymbol{\rho}}$, $\boldsymbol{\rho}_0$, $\boldsymbol{\rho}_N$	=	vectors containing the local elemental Cartesian degrees of freedom, the natural rigid body modes, and the natural straining modes
$\rho_{01}, \rho_{02}, \rho_{03}$	=	translational rigid-body mode along local elemental axis x', axis y', and axis z'
$\rho_{04}, \rho_{05}, \rho_{06}$	=	rotational rigid-body mode with respect to the local elemental axis x', axis y', and axis z'
ρ_{N1}	=	natural extensional straining mode
ρ_{N2}	=	natural symmetrical bending mode in the local $x'z'$ coordinate
ρ_{N3}	=	natural antisymmetrical bending mode in the local $x'z'$ coordinate
ρ_{N4}	=	natural symmetrical bending mode in the local $x'y'$ coordinate
ρ_{N5}	=	natural antisymmetrical bending mode in the local $x'z'$ coordinate
ρ_{N6}	=	natural torsional straining mode
$\boldsymbol{\sigma}$	=	stress vector

I. Introduction

MODERN engineering structures often operate at oscillating temperatures. Dynamic temperatures are not easily reproduced in the laboratory. Therefore, computer simulations must be conducted to obtain the dynamic response of such systems under the action of periodic heat loads.

It has been shown[1] that when isotropic and composite plates and shells are stressed thermally they exhibit irregular and chaotic behavior. The results were further analyzed[2] where the chaotic nature of the oscillations were mathematically proven and the existence of chaos formally established. Nonlinear free vibrations of composite plates also exhibit chaotic characteristics.[3] In particular, in-plane oscillations of small magnitude obey chaotic trends. Most studies, however, are concerned with systems comprising few degrees of freedom, the solution of which is based on differential equations. Therefore, there is a need for numerical studies on structures with many degrees of freedom. Also, there are no computational simulations that account for temperature effects.

The present study considers an isotropic semicircular arc under oscillating temperature. The time-dependent problem is solved,

Received 2 January 2002; revision received 29 June 2002; accepted for publication 29 June 2002.

*Research Scientist, Laboratory of Mechanics and Materials, Polytechnic School, Box 468; ltenek@yahoo.com. Member AIAA.

and the dynamic response is obtained. Two- and three-dimensional attractors are illustrated. The chaotic nature of the motion is proved mathematically. Computer plots indicate the structural deformation at two time instances.

II. Physical and Mathematical Model

The equilibrium state of a discretized system of forces in an inertial system is prescribed by the fundamental equation of dynamics[4]

$$\boldsymbol{R}_I + \boldsymbol{R}_D + \boldsymbol{R}_E = \boldsymbol{R} + \boldsymbol{J} \tag{1}$$

The principle of virtual work in dynamics is[4]

$$\int_V \rho \ddot{u}^t \delta u \, \mathrm{d}V + \int_V \sigma^t \delta\gamma \, \mathrm{d}V + \int_V \boldsymbol{p}^t_{VD} \delta u \, \mathrm{d}V = \int_V \boldsymbol{p}^t_S \delta u \, \mathrm{d}S + \boldsymbol{R}^t \delta r \tag{2}$$

In this work, we assume that all quantities are independent of temperature. By means of the finite element method, Eq. (2) is applied to every finite element in a structural system. By the invokation of standard finite element procedures, Eq. (2) in a global coordinate system yields the matrix equation[1,4]

$$M\ddot{r} + C\dot{r} + Kr = \boldsymbol{R} + \boldsymbol{J} \tag{3}$$

The stiffness matrix K is the sum of the two matrices, namely,

$$K = K_E + K_G \tag{4}$$

In concert with the natural-mode finite element method,[5] the beam finite element is assigned a set of rigid-body and straining modes. The beam finite element in space has 12 degrees of freedom (6 per node), and it can move as a rigid body in 6 possible modes, the rigid-body modes $\boldsymbol{\rho}_0$. In addition, if we subtract the 6 rigid-body modes from the 12 Cartesian degrees of freedom, we are left with 6 degrees of freedom, the natural straining modes $\boldsymbol{\rho}_N$ (Refs. 5 and 6). Formally, the natural mode vector comprises the entries

$$\boldsymbol{\rho} = \{\rho_0 \quad \rho_N\} \tag{5}$$

The rigid-body modes include three translations and three rotations in space that are grouped in the vector[5,6]

$$\boldsymbol{\rho}_0 = \{\rho_{01} \quad \rho_{02} \quad \rho_{03} \quad \rho_{04} \quad \rho_{05} \quad \rho_{06}\} \tag{6}$$

The rigid-body modes correspond to rigid-body force and moment components of the vector

$$\boldsymbol{P}_0 = \{P_{01} \quad P_{02} \quad P_{03} \quad P_{04} \quad P_{05} \quad P_{06}\} \tag{7}$$

The six straining modes include the extension, two symmetrical and two antisymmetrical bending modes, and a torsional mode. They are grouped in the vector[5,6]

$$\boldsymbol{\rho}_0 = \{\rho_{N1} \quad \rho_{N2} \quad \rho_{N3} \quad \rho_{N4} \quad \rho_{N5} \quad \rho_{N6}\} \tag{8}$$

and the natural forces are grouped in the vector

$$\boldsymbol{P}_N = \left\{F_N \quad M^1_S \quad M^1_A \quad M^2_S \quad M^2_A \quad M_T\right\} \tag{9}$$

The connection between the natural straining modes and the local nodal degrees of freedom is given by the relation

$$\boldsymbol{\rho}_N = \bar{a}_N \bar{\boldsymbol{\rho}} \tag{10}$$

The connection matrix $\bar{a}_N$ contains only zeros, ones, and geometrical parameters. All elemental matrices are given in Refs. 5 and 6.

In the presence of temperature, we shall assume a linear temperature distribution through the thickness, namely,

$$T(s, z') = T_0(s) + z' T_1(s) \tag{11}$$

This temperature field produces a constant temperature gradient. The parameters T_0 and T_1 are related to the temperatures at the top and bottom of a beam. The natural thermal load vector is written as the sum of two vectors, namely,[5,6]

$$\boldsymbol{J}_N = \boldsymbol{J}_{N0} + \boldsymbol{J}_{N1} \tag{12}$$

The natural load due to temperature is transformed to the global Cartesian coordinate via

$$\boldsymbol{J} = a^t_N \boldsymbol{J}_N \tag{13}$$

Global dynamic equilibrium is now established.

III. Computational Model

The beam finite element BEC is used to discretize the arc structure.[5,6] We now briefly describe the strategy to solve the nonlinear thermal dynamic problem. First, at time t_0, the user defines the initial displacement and velocities $\boldsymbol{r}_0$ and $\mathrm{d}r/\mathrm{d}t$. The problem proceeds by computing the initial accelerations, as well as the acceleration derivatives, namely,[3,4]

$$\boldsymbol{r}_{0,tt} = M^{-1}\left[\boldsymbol{R}(0) + \boldsymbol{J}(0) - C r_{0,t} - \boldsymbol{R}_e(\boldsymbol{r}_0)\right] \tag{14}$$

$$\boldsymbol{r}_{0,ttt} = M^{-1}\left[\boldsymbol{R}_{,t}(0) + \boldsymbol{J}_{,t}(0) - C r_{0,tt} - K(\boldsymbol{r}_0)\boldsymbol{r}_{0,t}\right] \tag{15}$$

Initialization of the initial accelerations, as well as the acceleration derivatives, follows, that is,

$$\boldsymbol{r}_{k,tt} = \boldsymbol{r}_{k-1,tt} + \Delta t \boldsymbol{r}_{k-1,ttt} \tag{16}$$

$$\boldsymbol{r}_{k,ttt} = \boldsymbol{r}_{k-1,ttt} \tag{17}$$

This information is passed to the predictor phase of the algorithm for predicting displacements and velocities, via[3,4]

$$\boldsymbol{r}_k = \boldsymbol{r}_{k-1} + \Delta t \boldsymbol{r}_{k-1,t} + (\Delta t^2/60)\left(21\boldsymbol{r}_{k-1,tt} + 3\Delta t \boldsymbol{r}_{k-1,ttt} + 9\boldsymbol{r}_{k,tt} - 2\Delta t \boldsymbol{r}_{k,ttt}\right) \tag{18}$$

$$\boldsymbol{r}_{k,t} = \boldsymbol{r}_{k-1,t} + (\Delta t/12)\left(6\boldsymbol{r}_{k-1,tt} + \Delta t \boldsymbol{r}_{k-1,ttt} + 6\boldsymbol{r}_{k,tt} - \Delta t \boldsymbol{r}_{k,ttt}\right) \tag{19}$$

The predictor phase proceeds with an inner loop over finite elements to compute and assemble all elemental matrices. There follow a series of computations of quantities: natural displacement increment $\rho_{N\Delta}$, natural forces $\boldsymbol{P}_N$, external forces $\boldsymbol{R}$, elastic stiffness k_E, geometric stiffness k_G, tangent stiffness K, mass matrix M, damping matrix C, and thermal load vector $\boldsymbol{J}$.

The next phase includes the corrector phase, which corrects the acceleration and the acceleration derivatives via

$$\boldsymbol{r}^c_{k,tt} = M^{-1}\left[R_k + J_k - C r_{k,t} - \boldsymbol{R}_e(r_k)\right] \tag{20}$$

$$\boldsymbol{r}^c_{k,ttt} = M^{-1}\left[R_{k,t} + J_{k,t} - C r_{k,tt} - K(r_k) r_{k,t}\right] \tag{21}$$

At this point, a decision over convergence must be made by invoking the norm

$$\frac{\left\|\boldsymbol{r}^c_{k,ttt} - \boldsymbol{r}_{k,ttt}\right\|}{\left\|\boldsymbol{r}_{k,ttt}\right\|} \le \varepsilon \tag{22}$$

If the convergence criterion (22) is satisfied, we set

$$\boldsymbol{r}^c_{k,tt} \to \boldsymbol{r}_{k,tt}, \qquad \boldsymbol{r}^c_{k,ttt} \to \boldsymbol{r}_{k,ttt} \tag{23}$$

and proceed to the next time step. If the convergence criterion (22) is not satisfied, we also utilize relations (23) and proceed to the predictor phase. This procedure is repeated until all time steps are completed. Note that the dynamic algorithm is an unconditionally stable implicit scheme.[3,4] The computational advances of the natural-mode finite element method are ensured.[7]

IV. Computational Experiments

Figure 1 shows an isotropic semicircular arc. All of the geometrical and material properties are given in the caption of Fig. 1. The arc can deform in three dimensions. It is subjected to its critical temperature augmented by a slight sinusoidal temperature using a frequency of 80 Hz. The radius-over-height of the arc is equal to 50. Its critical temperature is equal to $T = 0.895$°C. The computation advanced to $t = 0.0175$ s with a time step equal to $\Delta t = 1 \times 10^{-5}$ s and up to time to $t = 0.02575$ s with a time

step equal to $\Delta t = 1 \times 10^{-6}$ s. Note that a smaller time increment is computationally expensive, whereas a bigger time increment may fail to capture the structural behavior during this very fast dynamic phenomenon and also may introduce convergence problems. Time-displacement curves of the center point A are provided in Fig. 2. At a time of approximately 0.017 s, the arc starts to deform in large displacements. The curves reveal highly oscillatory movements. Figure 3 shows the three displacement curves up to time 0.015 s. It is observed that the horizontal displacement of point A (the u displacement) is extremely oscillatory. It is evident that the structure oscillates in the horizontal direction. There is little movement in the transverse y direction, while mild oscillatory behavior is taking place in the z direction. Figure 4 presents the trajectory of the motion of point A. Therein shown is the initial position and the motion of the central point in the u–w plane. In a similar manner, Fig. 5 shows the motion of central point A in the transverse v–w plane. Figure 6 shows the forming attractor of the vertical displacement and velocity of central point A. The attractor is evidently chaotic. Figure 7 shows the three-dimensional attractor of the vertical displacement, velocity, and acceleration of point A, respectively. Initially, the three-dimensional attractor is rather harmonic, but eventually chaotic patterns develop. Figure 8 shows a fast Fourier transform (FFT) of the velocity of point A. We observe from Fig. 8 that higher harmonic frequencies are present everywhere along the frequency spectrum. It is well known that the continuous presence of higher frequencies is indicative of chaos.[8–10] Figure 9 shows the Lyapunov exponent of the vertical central acceleration over an evolution time. The largest Lyapunov exponent shows the overall behavior of the system over an evolution time. The existence of a largest positive Lyapunov exponent confirms the inherent existence of chaos.[8–10] In the present study, the largest Lyapunov exponent is computed using the algorithm presented in Ref. 11. Figure 9 shows a positive Lyapunov exponent, and therefore, substantiation of chaos

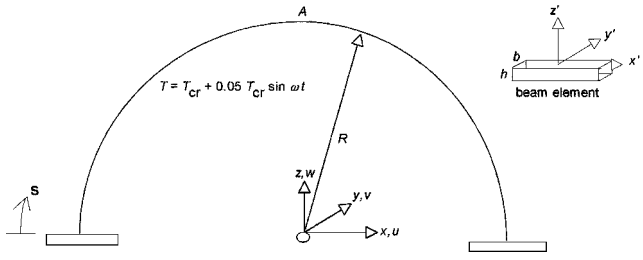

Fig. 1 Semicircular arc with $E = 90$ GPa, $R = 0.125$ m, $\nu = 0.3$, $h = b = 0.00250$ m, $\alpha_t = 25 \times 10^{-6}\,^{\circ}\mathrm{C}^{-1}$, $\omega = 80$ Hz, $T_{cr} = 0.895^{\circ}$C, and $\rho = 2700$ kg/m^3.

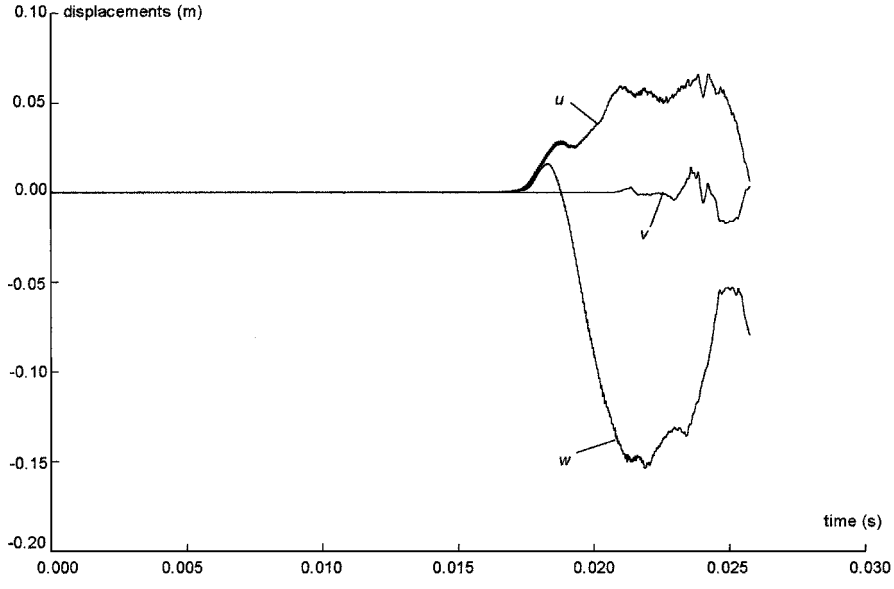

Fig. 2 Time-displacement curves for central point A up to $t = 0.02575$ s.

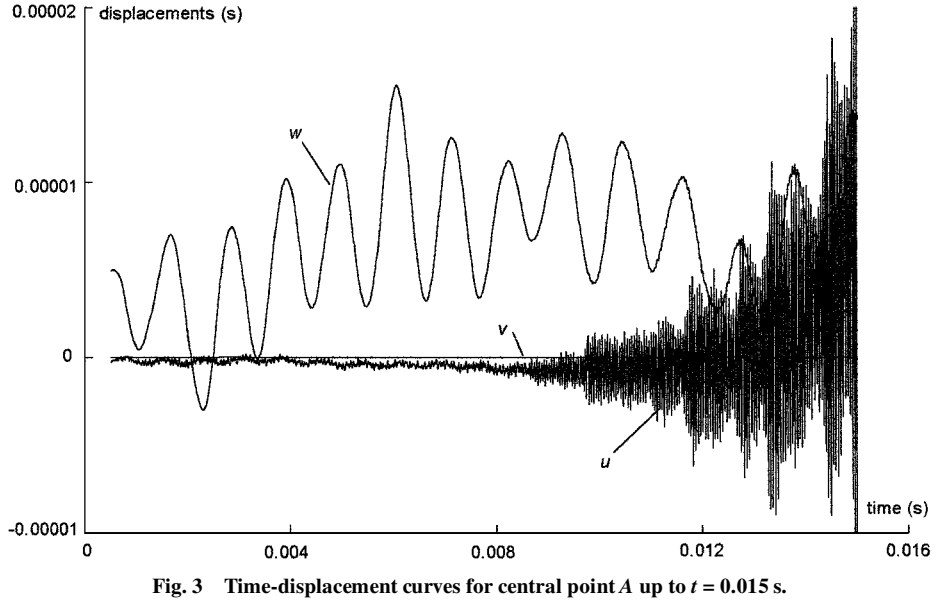

Fig. 3 Time-displacement curves for central point A up to $t = 0.015$ s.

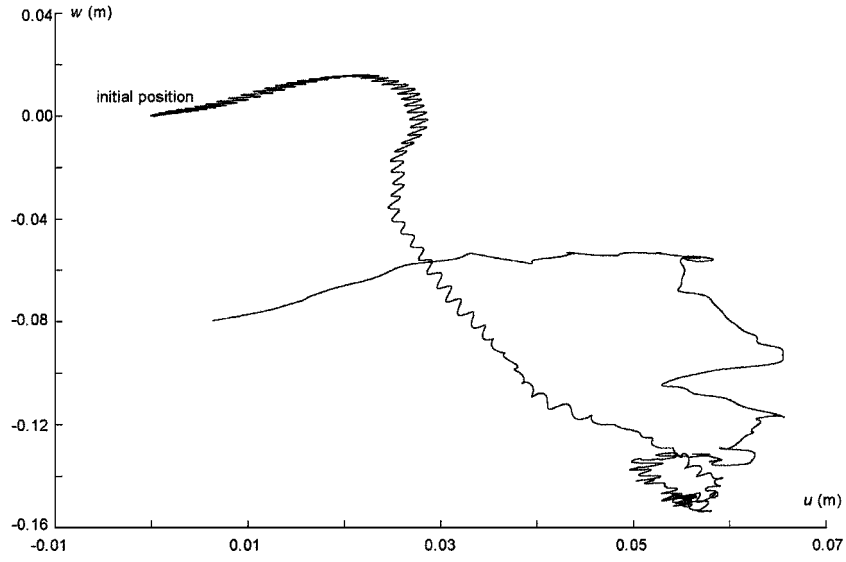

Fig. 4 Trajectory of central point A in u–w plane.

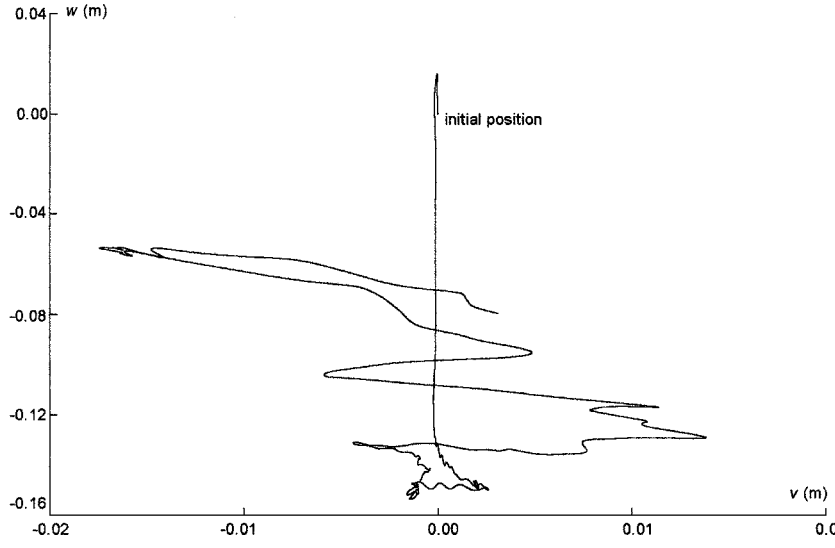

Fig. 5 Trajectory of central point A in v–w plane.

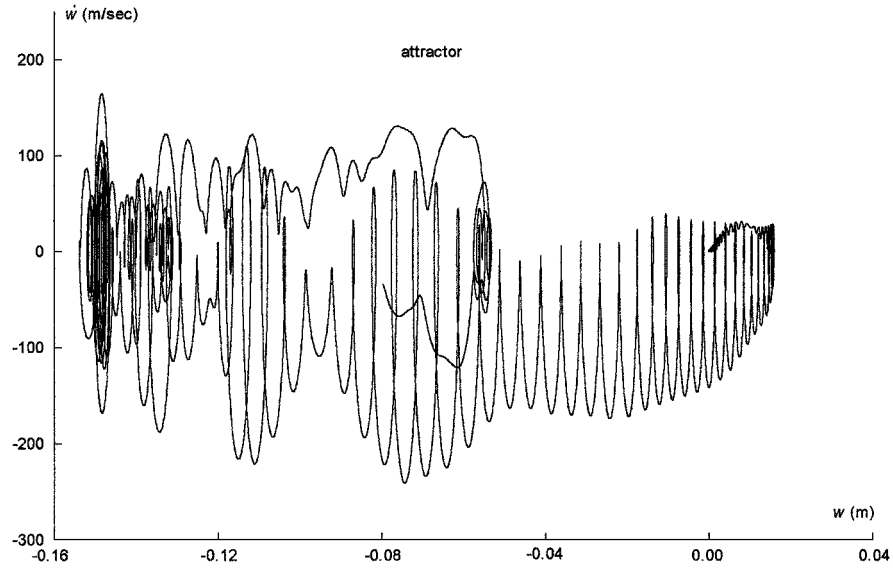

Fig. 6 Two-dimensional chaotic attractor of the vertical displacement of point A.

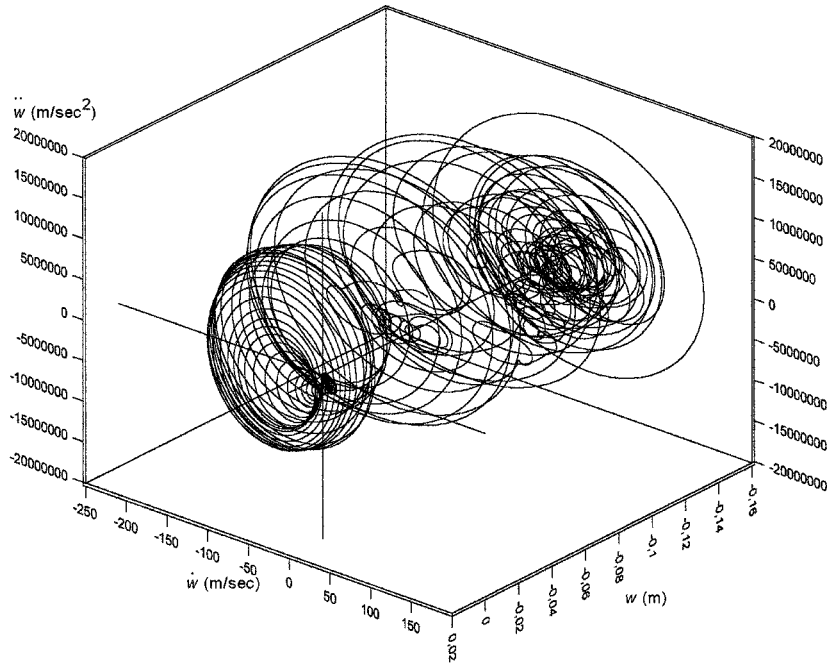

Fig. 7 Three-dimensional chaotic attractor of the vertical displacement of point *A*.

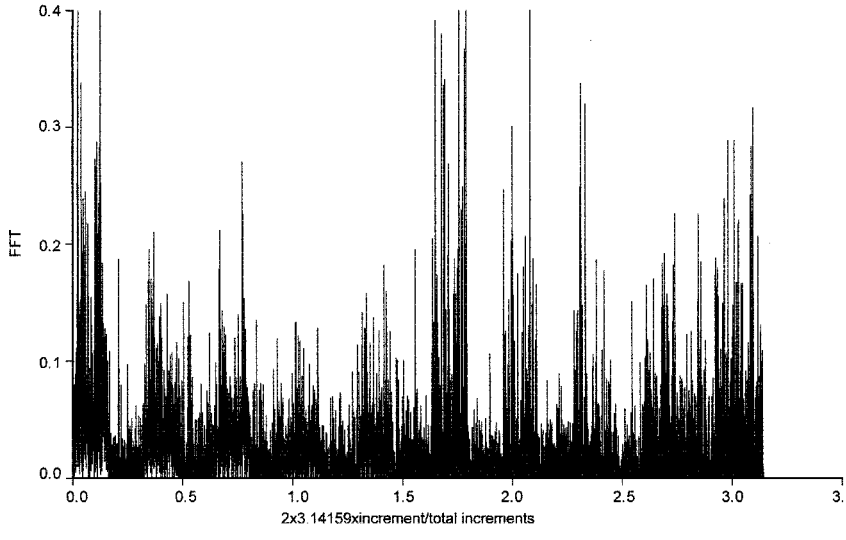

Fig. 8 FFT of the velocity of the central point *A*.

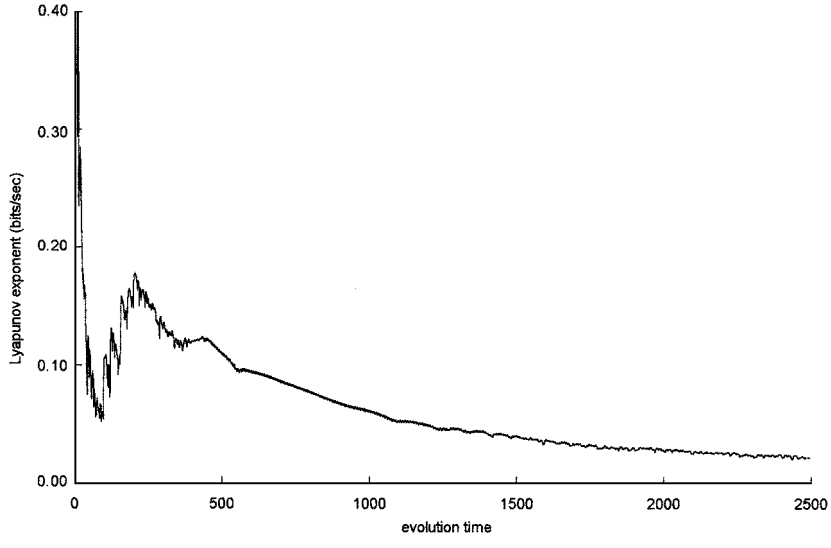

Fig. 9 Lyapunov exponent of the acceleration of central point *A*.

Fig. 10 Deformation of arc at $t = 0.02075$ s.

Fig. 11 Deformation of arc at $t = 0.02570$ s.

is formally established. Figure 10 shows the deformation of the arc at $t = 0.02075$, and Fig. 11 shows the structural deformation at $t = 0.0257$ s. Figure 11 shows a possible catastrophic collapse of the space arc.

V. Conclusions

A three-dimensional isotropic space arc is dynamically thermally stressed with a temperature equal to its critical temperature plus a small sinusoidal time increment. From the onset of the vibration, highly irregular oscillations occur. Following the initial vibration period, chaotic oscillations develop. Then, the arc structure vibrates with very large displacements in a chaotic manner. Two- and three-dimensional attractors substantiate the existence of chaos. The FFT and the value of the Lyapunov exponent formally prove the existence of chaos. Computer plots (Figs. 10 and 11) illustrate the structural deformation.

References

[1]Argyris, J., and Tenek, L., "Nonlinear and Chaotic Oscillations of Composite Plates and Shells Under Periodic Heat Load," *Computer Methods in Applied Mechanics and Engineering*, Vol. 122, 1995, pp. 351–377.

[2]Argyris, J., Tenek, L., Andreadis, I., Athanasiou, M., and Pavlos, G., "On Chaotic Oscillations of a Laminated Composite Cylinder Subject to Periodic Application of Temperature," *Chaos, Solitons and Fractals*, Vol. 9, No. 9, 1998, pp. 1529–1554.

[3]Argyris, J., Tenek, L., and Olofsson, L., "Nonlinear Free Vibration of Composite Plates," *Computer Methods in Applied Mechanics and Engineering*, Vol.122, 1994, pp. 1–51.

[4]Argyris, J., and Mlejnek, H. P., *Dynamics of Structures*, Elsevier, North-Holland, Amsterdam, 1991.

[5]Tenek, L., and Argyris, J., *Finite Element Analysis for Composite Structures*, Kluwer Academic, Dordrecht, The Netherlands, 1998.

[6]Argyris, J., Tenek, L., and Mattsson, A., "BEC: A 2-Node Fast Converging Shear-Deformable Isotropic and Composite Beam Element Based on 6 Rigid-Body and 6 Straining Modes," *Computer Methods in Applied Mechanics and Engineering*, Vol. 152, 1998, pp. 281–336.

[7]Tenek, L., and Argyris, J., "Computational Aspects of the Natural-Mode Finite Element Method," *Communications in Numerical Methods in Engineering*, Vol. 13, 1997, pp. 705–713.

[8]Tsonis, A. A., *Chaos from Theory to Applications*, Plenum, New York, 1992.

[9]Moon, F. C., *Chaotic and Fractal Dynamics: An Introduction for Applied Scientists and Engineers*, Wiley, New York, 1992.

[10]Argyris, J., Faust, G., and Haase, M., *An Exploration of Chaos*, Elsevier, North-Holland, Amsterdam, 1994.

[11]Wolf, A., Swift, J. B., Swinney, H. L., and Vastano, J., "Determining Lyapunov Exponents from a Time Series," *Physica D*, Vol. 16, 1985, pp. 285–317.

A. Berman
Associate Editor